JOURNAL OF CATALYSIS 138, 283–293 (1992)

Microstructures of Pt–Ce and Rh–Ce Particles on Alumina and Silica[1]

J. M. SCHWARTZ[2] AND L. D. SCHMIDT[3]

Department of Chemical Engineering and Materials Science, University of Minnesota, Minneapolis, Minnesota 55455

Received February 4, 1992; revised May 12, 1992

The effects of adding Ce to 20–200 Å diameter particles of Pt and Rh on planar Al_2O_3 and SiO_2 substrates are examined using transmission electron microscopy (TEM), X-ray photoelectron spectroscopy (XPS), and electron energy-loss spectroscopy (EELS), following treatments in H_2 and O_2 atmospheres. Samples were transferred repeatedly between furnace and TEM so that the time evolution of the microstructure of individual particles could be followed. TEM shows that upon heating Pt alone on Al_2O_3 or SiO_2 in H_2, Pt forms cubic particles, while when Pt and Ce are codeposited, the Pt particles are about the same size but no longer have square outlines. XPS shows that the Pt peak shifted to Pt^{+2} when heated in O_2 on both Al_2O_3 and SiO_2 when Ce was present and returned to Pt^0 after heating in H_2. The Pt particles tend to shrink or disappear after heating in O_2 at 650°C, and this is much faster without Ce, showing that Ce retards the volatilization of Pt oxides. When Rh–Ce on Al_2O_3 of SiO_2 is heated in H_2, Rh forms particles of no preferred shape. After heating in O_2 to 600°C, Rh oxidizes to Rh_2O_3 and remains particulate on Al_2O_3, but spreads to a film on SiO_2 in the presence of Ce. Upon reduction, Rh_2O_3 reduces to metallic Rh and forms particles of approximately the same size as the original particles on Al_2O_3 and larger than the original size on SiO_2. $Ce_2Si_2O_7$ has been characterized on SiO_2 adjacent to Rh particles after reduction of an oxidized sample, but $CeAlO_3$ has not been observed on Al_2O_3.

INTRODUCTION

Cerium is added as a promoter to noble metals in the automotive catalytic converter. Several possible mechanisms of this promotion have been suggested, such as Ce preventing sintering of the catalyst particles, increasing the dispersion of the catalyst (*1*), providing oxygen storage by shifting between Ce_2O_3 under fuel-rich conditions and CeO_2 under fuel-lean conditions (*2–4*), promoting the water–gas shift reaction (*5, 6*), and stabilizing the alumina support (*7*).

Cerium is typically present as either Ce^{+3} or Ce^{+4}. CeO_2 is the most stable form of Ce^{+4} in neutral or oxidizing atmospheres. Ce^{+3}, the most commonly observed reduced form, includes compounds such as Ce_2O_3 and $Ce_2Si_2O_7$, which have been observed using TEM for Rh–Ce on SiO_2 (*8*), and $CeAlO_3$, which has been reported for alumina supported catalysts following heating in H_2 at high temperatures (*9*). Both Pt and Pd have been shown to promote the reduction of CeO_2 to Ce_2O_3 in H_2 or CO and also to promote the reoxidation back to CeO_2 by O_2 (*10*). Pt_5Ce has been reported in Pt–Ce/Al_2O_3 catalysts following heating in H_2 at 900°C (*1*). A Pt–Ce intermetallic compound has also been proposed for Pt/CeO_2 catalysts following high-temperature reduction (*11*). A Pt–Al alloy has also been reported for Pt/Al_2O_3 catalysts following treatments in hydrogen at high temperature (>500°C) (*12*).

We have examined both the Pt–Ce and Rh–Ce systems on planar γ-Al_2O_3 thin films using transmission electron microscopy

[1] This research was partially supported by NSF under Grant CBT-882745 and by a grant from Ford Motor Company.

[2] Supported by Amoco Fellowship.

[3] To whom correspondence should be addressed.

0021-9517/92 $5.00

(TEM). We contrast these results with previous results on amorphous SiO_2 (*8, 13*), where platinum formed cubes when heated in H_2 without Ce present and more rounded shapes of approximately the same size when Ce was present. Heating in O_2 caused the Pt particles to become more rounded and smaller. After an initial reduction, Rh on SiO_2 formed metallic particles and Ce was present as an amorphous film. Heating in O_2 caused the Rh_2O_3 to spread on the SiO_2 surface and crystalline CeO_2 particles to form. Further reduction caused larger Rh particles to form than were initially present and the CeO_2 to return to an amorphous film. We also examined both of these systems chemically using electron energy spectroscopy (EELS) and X-ray photoelectron spectroscopy (XPS) with the metal catalyst and cerium deposited on films of alumina or silica (*8*). We showed using XPS and EELS that Ce alternates between Ce^{+3} following heating in H_2 and Ce^{+4} after heating in O_2 while Rh switches between Rh^0 and Rh^{+3} on SiO_2. We also used high-resolution TEM to show the existence of $Ce_2Si_2O_7$ adjacent to Rh particles on Rh–Ce/SiO_2 after extensive reduction following oxidation, and that $Ce_2Si_2O_7$ was stable even in oxidizing atmospheres at elevated temperatures.

We use TEM to observe the microstructures of the same particles after heating planar samples in H_2 and in O_2 at atmospheric pressure for several hours. These conditions are more extreme, but for shorter times than the actual catalyst would encounter, so we would expect the changes in real catalysts to be somewhat different than we observed here. Using EELS, we can examine very small areas ~30 Å in diameter or larger areas of the TEM sample in the microscope and observe chemical shifts for Ce. XPS is highly surface sensitive and gives chemical shifts but has no lateral resolution.

EXPERIMENTAL

TEM samples were prepared by depositing Pt or Rh and Ce on thin planar films of γ-Al_2O_3 or SiO_2, similar to techniques described previously (*13*). Al_2O_3 and SiO_2 films were prepared by vacuum evaporation of ~200 Å of Al or Si onto a Formvar film which had been deposited on a gold microscope grid. The grid was then heated in O_2 to oxidize the Al or Si and burn off the Formvar. This produced a uniform film of crystalline γ-Al_2O_3 or amorphous SiO_2. Thin films of about 30 Å of Pt or Rh were then deposited by vacuum evaporation and heated in H_2 at 650°C to produce particles. Ce was also added by vacuum evaporation of a thin film followed by heating in H_2. In some experiments metal and Ce were deposited on halves of the grid by masking the other half of the grid during evaporation. Using this technique, it was possible to have *different metal and Ce loadings on the same microscope grid*, which allows for direct comparison of different compositions (*13*).

TEM was performed in a Philips CM30 microscope. EELS was performed in the microscope using a Gatan model 666 spectrometer with a 1024-channel photodiode array for parallel detection of the spectrum. Typical spectra were acquired in 5–10 min. For an incident electron beam energy of 300 keV, the energy resolution was less than 2 eV FWHM using entrance apertures to the spectrometer for sample areas from 30 to 3000 Å in diameter.

XPS samples on planar SiO_2 supports were prepared by heating Si wafers in O_2 to oxidize the surface of the wafer. XPS samples with Al_2O_3 supports were prepared by vacuum evaporating ~200 Å of Al onto a Si wafer and heating in O_2 to oxidize the Al. Pt, Rh, and Ce were then vacuum evaporated onto these samples. XPS spectra were acquired using a Perkin–Elmer 5400 spectrometer. Peak energies were calibrated relative to carbon which was assumed to be 284.6 eV.

Samples were heated in flowing H_2 or O_2 in a tube furnace at atmospheric pressure. Typical conditions were heating in H_2 at 650°C followed by heating in O_2 and further heating in H_2 at gas flow rates of ~50 cc/min. Before analysis, samples were exposed

to ambient air after cooling following each heat treatment. This could have affected our results since oxidation of cerium is possible in ambient air. We show here sequences from single samples, but all results were repeated on several different samples with results consistent with those shown.

RESULTS

Microstructure of Pt–Ce

Figure 1 shows TEM micrographs of Pt with and without Ce on an Al_2O_3 support following heat treatments in H_2 and O_2 at 650°C for 6 hr. Figures 1a and 1b show the same region from the half of the grid without Ce, while 1c and 1d show the same area from a different region on the other half of the same grid with Ce present. Figures 1a and 1c show the microstructures after heating in H_2, while 1b and 1d show the microstructures of the same areas following heating in O_2. The arrows point to the same particles on each sample.

As seen in Figs. 1a and 1c, Pt forms cube shaped particles ~100 Å in diameter on Al_2O_3 when heated in H_2 both with and without the presence of Ce. The corners of the cubes are typically sharper when there is no Ce present. The sizes of the Pt particles do not appear to be altered by Ce, but there are more defects in the Pt particles when Ce is present. This is consistent with our previous observations of Pt–Ce on SiO_2 (*13*). The presence of Ce does not alter the lattice constant of Pt, and there was no evidence of any Pt–Ce compounds. Electron diffraction shows some crystalline CeO_2 on Al_2O_3 although distinct CeO_2 particles are not visible. This differs from our previous observations on SiO_2 in which no crystalline CeO_2 was detected after heating in H_2 (*8*).

The most dramatic effect of Ce with Pt occurs after heating to high temperatures (650°C) in O_2. As seen in Fig. 1d, there is clearly some Pt remaining on the section where Ce was also deposited, although some particles are smaller or have disappeared. The region without Ce shows almost no Pt remaining after heating in O_2. EELS and energy dispersive spectroscopy (EDS) were used to confirm that there is no Pt remaining in the regions where it is not visible. From these micrographs it is evident that *Ce inhibits the loss of Pt* from the Al_2O_3 sample. This also occurs on SiO_2. The remaining Pt particles in Fig. 1d do not have sharp corners.

Microstructure of Rh–Ce

Figure 2 shows the microstructures of Rh–Ce on Al_2O_3 of the same area following sequential heat treatments in H_2, O_2, O_2 for longer time, and again in H_2. The arrows point to the same particles in the micrographs.

After heating in H_2 at 650°C for 6 hr (Fig. 2a), Rh is metallic and forms ~100-Å diameter particles of no preferred shape or orientation as previously observed on SiO_2 (*13*). The dark areas in the upper and lower left corners are from contrast in the alumina support and were used to locate the same area each time.

As expected, heating this sample in O_2 for 2 hr at 650°C (Fig. 2b) oxidizes the Rh, confirmed using XPS and electron diffraction (not shown), and breaks up the CeO_2 film into particles. Electron diffraction (not shown) confirms the presence of crystalline CeO_2. The Rh_2O_3 remains as particles of nearly the same size as the metallic Rh particles in Fig. 2a. Further heating in O_2 for 2 hr at 650°C (Fig. 2c) does not change the microstructure significantly from that in Fig. 2b.

After heating this sample in H_2 at 650°C for 10 hr (Fig. 2d), most of the CeO_2 returns to a film and the Rh_2O_3 reduces to Rh metal. The Rh particles are nearly the same size and in the same positions as they were in Fig. 2a. The crystalline CeO_2 particles which were visible in Figs. 2b and 2c have disappeared.

Figure 3 shows the microstructure of Ce and Rh–Ce on SiO_2 as discussed elsewhere (*8*). The microstructures of Rh–Ce on both supports are similar after an initial heating in H_2; the Rh is still present as metallic parti-

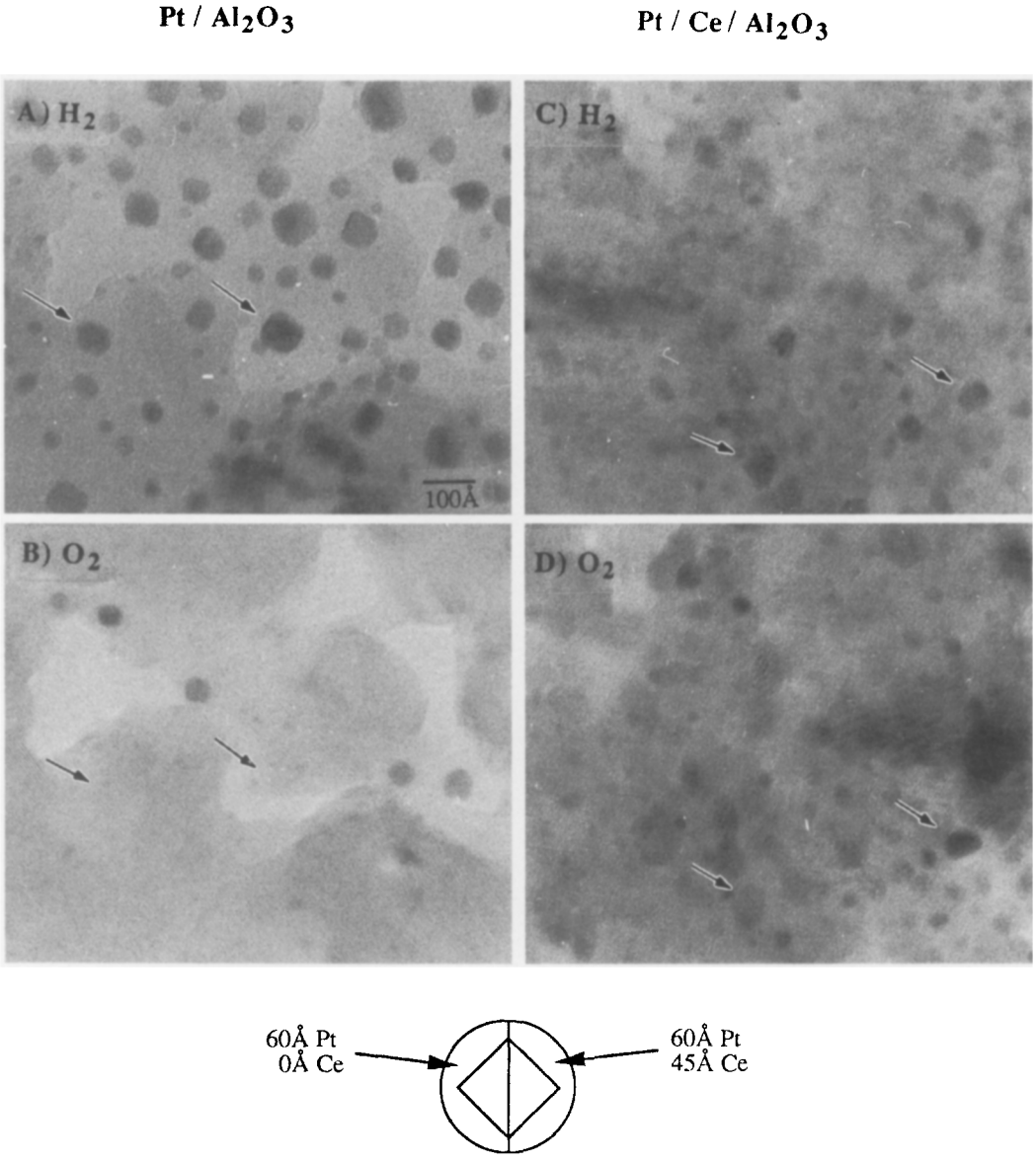

FIG. 1. TEM micrographs of Pt and Pt–Ce on alumina. Two regions with different loadings were prepared on the same TEM grid as sketched below. The upper micrographs show the microstructures after heating in H_2 at 650°C for 6 hr and the lower micrographs show the same areas after heating in O_2 for 6 hr at 650°C: (a) and (b) show a loading of 60 Å of Pt; (c) and (d) show a loading of 60 Å of Pt and 45 Å of Ce. Pt volatilizes when heated in O_2 when there is no Ce present. Ce inhibits the volatilization of Pt particles when heated in O_2.

cles of no preferred shape or orientation while Ce is present as an amorphous film.

However, there are significant differences between the microstructures on SiO_2 and Al_2O_3 supports following heating in O_2. On Al_2O_3, the Rh_2O_3 remained as particles in approximately the same positions as the metallic Rh particles. On SiO_2, however, *the Rh_2O_3 spreads on the surface as a thin film in the presence of Ce*. In contrast, Rh_2O_3

$Rh/Ce/Al_2O_3$

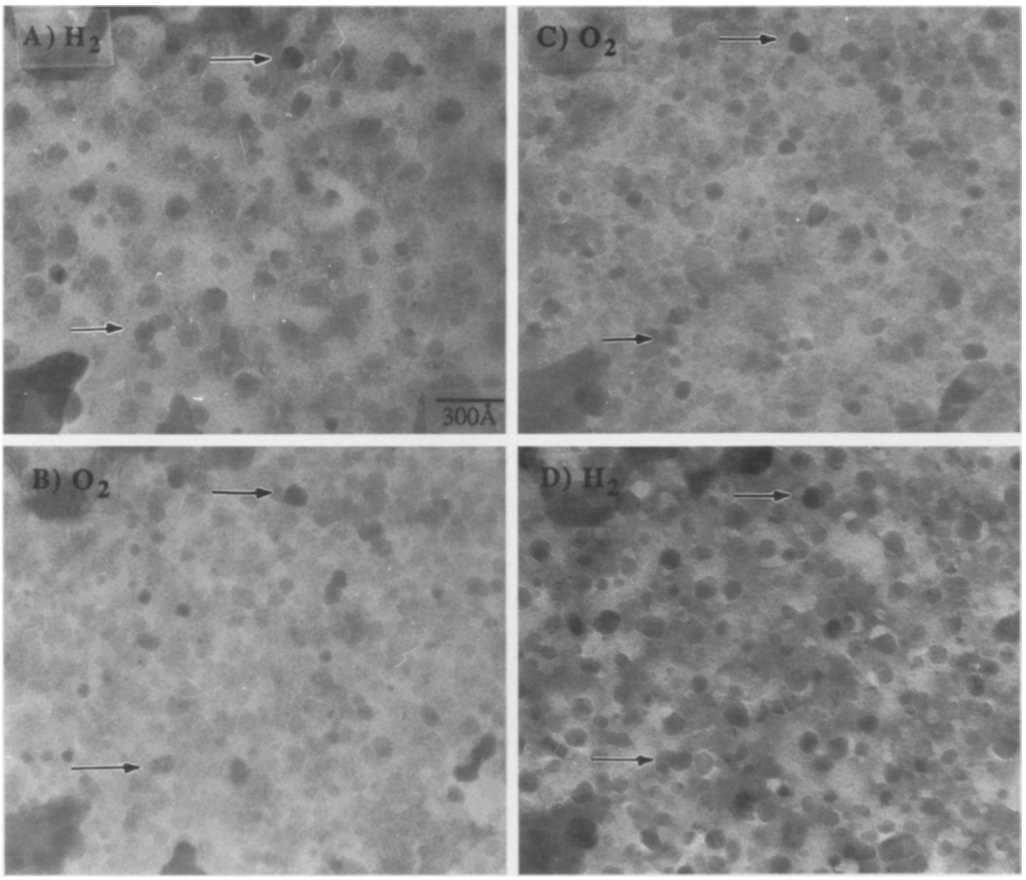

FIG. 2. TEM micrographs of Rh–Ce on alumina. All four micrographs are from the same area, with arrows identifying individual particles. The first micrograph, (a), shows the microstructures after heating in H_2 at 650°C for 6 hrs, (b) shows the same area after heating in H_2 for 2 hr, (c) is after heating in O_2 at 650°C for an additional 2 hr, and (d) is after heating in H_2 at 650°C for 10 hr. Rh_2O_3 does not spread on alumina as it does on silica. No $CeAlO_3$ is observed.

does not spread on either support when there is no Ce present. After oxidation, crystalline CeO_2 particles are visible on both supports.

Further heating of the oxidized samples in H_2 also demonstrates differences between the two supports. On Al_2O_3, the Rh_2O_3 particles were reduced to metallic Rh particles of approximately the same sizes and in the same positions as after the first H_2 treatment. On SiO_2, the Rh_2O_3 film was reduced and formed Rh particles that were larger than the original Rh particles and in different positions. This effect was observed only when Ce was present.

Oxidation and Reduction of Rh and Pt

XPS shows that Rh oxidizes to form Rh_2O_3 when heated in O_2 and reduces to form Rh^0 when heated in H_2 as expected. This occurs on both supports whether or not Ce is present. The measured binding energies for the $3d_{5/2}$ peak were 307.0 eV

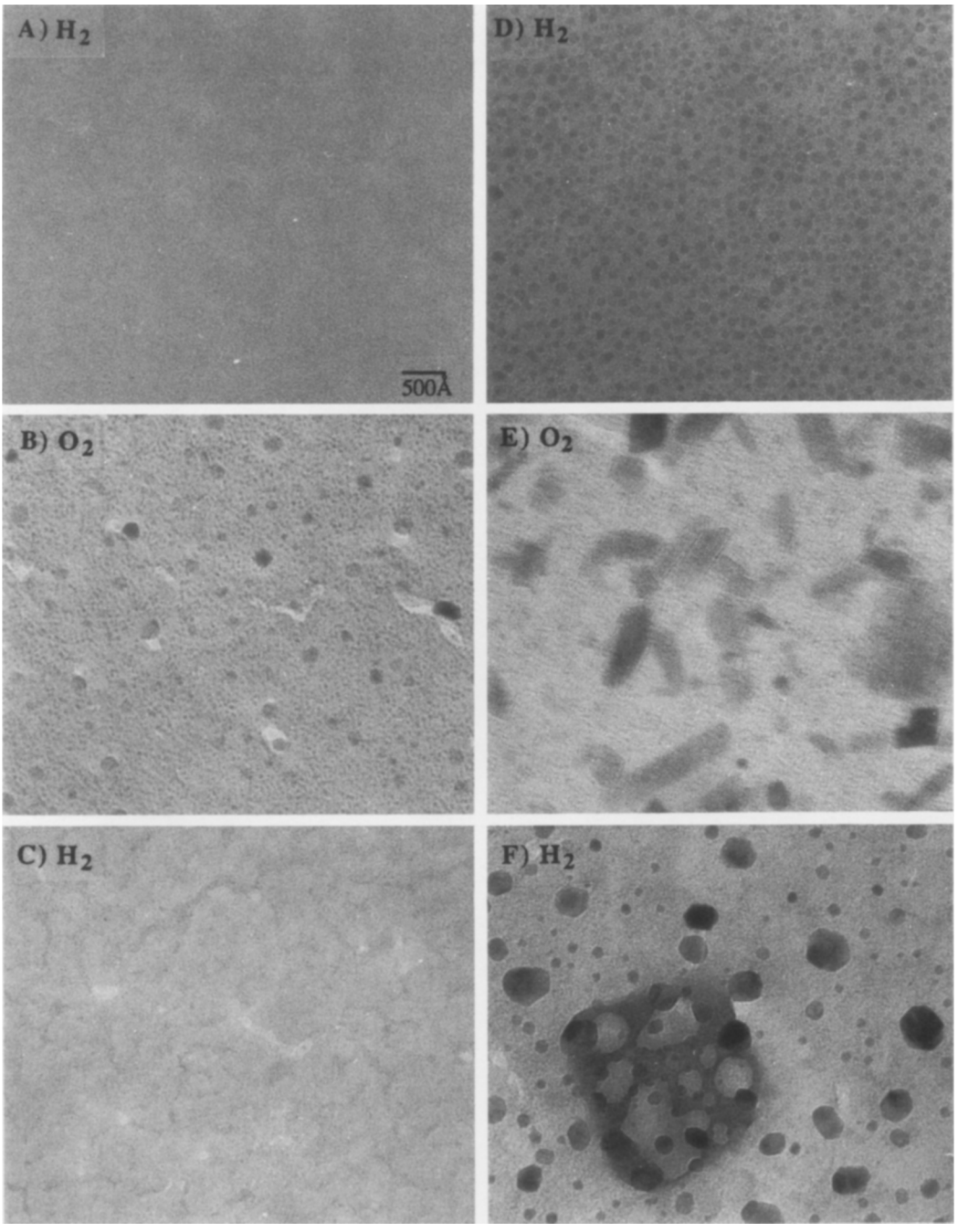

FIG. 3. TEM micrographs of Rh–Ce on silica. Two samples with different loadings were prepared on the same TEM grid. The top micrographs are after heating in H_2 at 600°C for 14 hr, the middle micrographs are after heating in O_2 at 600°C for 1 hr, and the bottom micrographs are after heating in H_2 again at 600°C for 4 hr. (a)–(c) show a loading of 14 Å of Ce. Ce forms a continuous amorphous film which becomes granular in O_2. (d)–(f) show loadings of 8 Å of Rh and 22 Å of Ce. The Ce forms many large CeO_2 particles after heating in O_2 and the Rh oxidizes and spreads on the SiO_2. Reduction in H_2 produces much larger Rh particles and patches of $Ce_2Si_2O_7$ adjacent to some Rh particles.

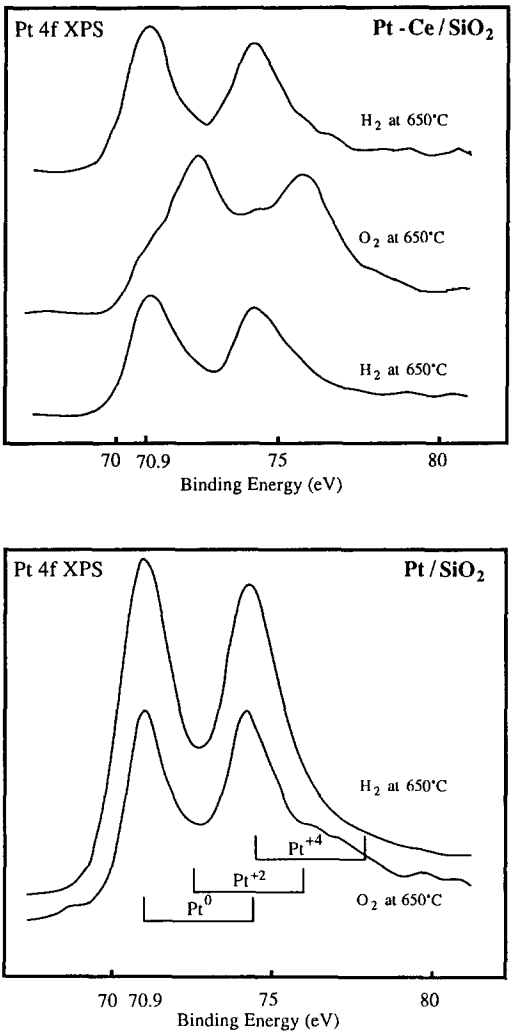

FIG. 4. Pt 4*f* XPS spectra (Pt–Ce on SiO_2 and Pt on SiO_2) during a sequence of treatments in H_2 and O_2. Both sets of spectra show that Pt is present as Pt metal after heating in H_2. Pt oxidizes to Pt^{+2} after heating in O_2 when Ce is present but remains Pt^0 after heating in O_2 without Ce. Further heating in H_2 reduces the oxidized Pt to Pt^0.

after heating in H_2 and 308.2 eV after heating O_2. Both of these values are in agreement with previously reported values for Rh^0 and Rh_2O_3 (*14*).

Figure 4 shows the XPS spectra of Pt on SiO_2 with and without Ce. Pt is in the metallic state after heating in H_2 whether or not Ce is codeposited. Pt does not shift when heated in O_2 when Ce is not present but shifts when there is Ce on either SiO_2 or Al_2O_3. On SiO_2 after heating in H_2, the Pt $4f_{7/2}$ peak had a binding energy of 70.9 eV, which is in agreement with reported values for Pt metal (*15*). However, after heating in O_2, the measured binding energy was 72.3 eV for the sample with Ce, which is in agreement with some reported values for PtO (*16–18*) but not in agreement with others (*19, 20*), as discussed later.

For Pt–Ce/Al_2O_3, the relative heights of the Pt and Al peaks show a definite loss of Pt from the sample without Ce after heating in O_2 which is due to volatilization of Pt oxides discussed previously. The shift in the Pt $4f_{7/2}$ peak to the binding energy of PtO when there is Ce on the sample is detectable on Al_2O_3, but the Pt 4*f* peak is convoluted with the Al 2*p* peak, making quantitative analysis more difficult. The Pt 4*d* signal, which is not convoluted with Al, was too weak to be usable.

Oxidation and Reduction of Ce

XPS and EELS were both used to study the oxidation states of Ce following different heat treatments. Figure 5 shows XPS spectra of Ce from samples with Pt on both supports. Figure 6 shows EELS spectra of Ce from samples with Rh on both supports. Ce behaves differently on the two supports. On SiO_2, both XPS and EELS show that Ce is present as a Ce^{+3} species after heating in H_2 followed by exposure to the ambient air at 25°C. On Al_2O_3, both EELS and XPS showed the presence of Ce^{+4} following heating in H_2 and subsequent exposure to the atmosphere at room temperature.

Heating both samples in O_2 caused the Ce to form CeO_2 on both supports. Further heating in H_2 caused both samples to return to their original states after heating in H_2, Ce^{+3} on SiO_2, and Ce^{4+} on Al_2O_3. The overall behavior of Ce was not affected by the presence of Pt or Rh on either support, although $Ce_2Si_2O_7$, a minor component, will not form if Pt or Rh is absent.

EELS showed the same oxidation and re-

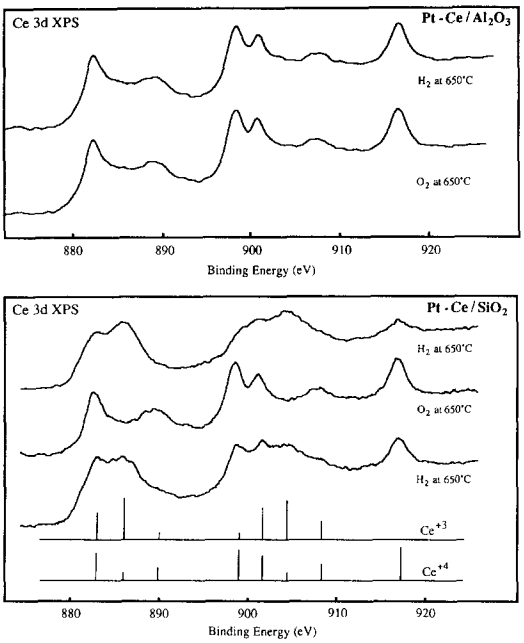

FIG. 5. Ce 3*d* XPS spectra (Pt–Ce on Al_2O_3 and Pt–Ce on SiO_2) during a sequential treatment in H_2 and O_2. Ce is present as Ce^{+4} on Al_2O_3 regardless of treatment while Ce is transformed between +3 and +4 valence states by heating in H_2 and O_2, respectively, on SiO_2.

duction behavior of Ce on TEM samples as was observed by XPS. EELS showed CeO_2 regardless of heat treatment on Al_2O_3 after exposure to the atmosphere. On SiO_2, EELS shows a shift between Ce^{+3} following heating in H_2 and exposure to the atmosphere and CeO_2 following heating in O_2. The Ce 3*d* edge has two sharp peaks called white lines which are the results of a high density of unfilled *f*-states (*21*). These white lines allow for accurate measurements of energy losses and chemical shifts. The high energy shoulder visible only in Ce^{+4} and the change in the relative heights of the two white lines are often more reliable indications of a chemical shift than a change in energy, which is subject to calibration errors.

DISCUSSION

Microstructure of Pt–Ce

Pt forms cubic particles on Al_2O_3 after heating in H_2 on either support when there is no Ce present. This is in agreement with our previous observations of Pt on SiO_2 (*22*). Others have also seen distinct (100) facets on micrometer-sized Pt droplets after heating in vacuum and concluded that although the anisotropy of the surface energies of different Pt planes is small under these conditions, the (100) plane has the lowest energy and that the environment can affect the particle shape (*23*). When Ce is codeposited, the Pt particles still tend to form cubes, but the corners are not as sharp. Evidently, Ce reduces the anisotropy of the energies of the various crystal planes of Pt in H_2, but the (100) plane is still energetically favored. Since catalytic activity generally increases on surfaces with lower coordination, it is possible that Ce increases the catalytic activity of Pt in some reactions by exposing higher index planes.

The loss of Pt from the sample as shown in Fig. 1 following heating in O_2 is most likely due to formation and volatilization of

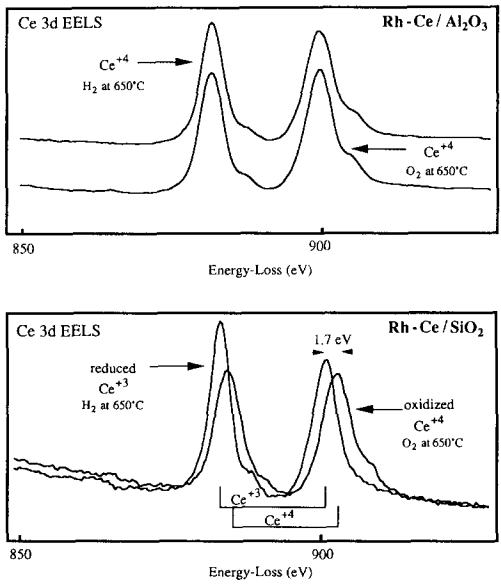

FIG. 6. Ce 3*d* EELS spectra acquired from large areas of Rh–Ce on Al_2O_3 (top) and SiO_2 (bottom) after initial reduction and oxidation at 650°C for 4 hr. No shift was observed on Al_2O_3, while a shift of 1.7 eV in white line energies was measured between the H_2 and O_2 treatments on SiO_2.

Pt oxide, PtO_2. XPS shows that Pt^{+2} can be stabilized by the presence of Ce, but Pt oxides volatilize more readily when there is no Ce present. This has been observed on both Al_2O_3 and SiO_2 supports. Heating in O_2 at 400–500°C did not oxidize Pt as shown by XPS and did not volatilize Pt particles as seen in TEM. Pt volatilization requires high temperatures and will occur when Ce is present, but to a much lesser extent than samples with no Ce. Thus, Ce stabilizes Pt oxides against volatilization at high temperatures.

A volatile oxide, PtO_2, forms upon heating Pt wire or foil in air or O_2 (*24, 25*). From measurements above 1100°C, the vapor pressure of PtO_2 at 650°C is approximately 10^{-10} atm as determined by extrapolating reported partial pressures of PtO_2 (*26*) using the Clausius–Clapeyron equation. This corresponds to a maximum evaporation rate of ~20 monolayers per hour assuming no redeposition, which is fast enough to account for the observed loss of Pt. The vapor pressure of Pt metal at 650°C, also found by extrapolation of reported vapor pressures (*27*), is about 10^{-24} atm, too low for any appreciable evaporation. The addition of Ce alters the vapor pressure of the platinum phase, probably by forming a compound between Pt and Ce with oxygen, from which the evaporation rate is much lower than PtO_2.

Microstructure of Rh–Ce

Unlike Pt–Ce, Rh–Ce behaves differently on the two supports. As shown in Fig. 3e, Rh_2O_3 spreads on SiO_2 when Ce is present but remains as Rh_2O_3 particles on Al_2O_3 as shown in Fig. 2b. An important consequence of the difference between the two supports is that the final size of the Rh particles on SiO_2 can be altered. Since the dispersion of Rh_2O_3 and subsequent sintering into Rh particles following reduction does not occur on Al_2O_3, the size of the particles is fixed by their original size and cannot be changed as easily as it can on SiO_2. The differences observed in the microstructure on the two supports are probably due to stronger interactions between the Rh and Rh_2O_3 with Al_2O_3 than with SiO_2.

Another significant difference in the behavior of Rh–Ce on the two supports is the formation of $Ce_2Si_2O_7$ on SiO_2, but the absence of $CeAlO_3$ on Al_2O_3. The large gray area in Fig. 3f has been identified as $Ce_2Si_2O_7$ using high-resolution TEM and discussed elsewhere (*8*). $Ce_2Si_2O_7$ does not form in regions of the TEM sample without Rh and is only seen adjacent to Rh particles. $Ce_2Si_2O_7$ and $CeAlO_3$ are both stable in air, so if $CeAlO_3$ were formed, we should be able to see it with TEM, EELS, or XPS. We have never observed Ce^{+3} as either Ce_2O_3 or $CeAlO_3$ on Al_2O_3 with Pt or Rh or alone.

Oxidation and Reduction of Rh and Pt

Rh remains metallic after heating in H_2 and oxidizes to Rh_2O_3 when heated in O_2 on either support. This agrees with our previously reported observations of Rh–Ce on SiO_2 (*8*). XPS results give the same binding energies for Rh^0 and Rh_2O_3 as previously reported (*14*). The same binding energies were found on Al_2O_3 as on SiO_2.

On SiO_2, there is a clear shift in the binding energy of Pt with Ce after heating in O_2 which indicates that there is oxidized Pt on the surface as well as metallic Pt, visible as shoulders. We believe that we have produced an amorphous Pt^{+2} species, most likely a form of PtO, by heating Pt–Ce samples in O_2, but we cannot conclusively identify the species because we are not able to distinguish between different phases of Pt^{+2} since we observe no diffraction rings. The binding energy of the Pt $4f_{7/2}$ peak was 70.9 eV after heating in H_2, in agreement with reported values for Pt^0 (*15*). The binding energy of the sample did not change after heating in O_2 without Ce. However, when Ce was also deposited on the sample, there was a shift in the Pt peak to 72.3 eV. Pt is known to exist as Pt^0, Pt^{+2}, or Pt^{+4} corresponding to Pt metal, PtO, and PtO_2. Literature values for PtO include 72.2 eV (*16*),

72.3 eV (*17, 18*), 73.3, eV (*19*), and 74.4 eV (*20*). Literature values for PtO_2 range from 73.6 eV (*18*) to 74.5 eV (*16*). We did not observe any shift to Pt^{+4}. The value reported by Kim would be 73.9 eV if scaled to 284.6 eV for C 1*s* since he used a different reference. The other references used agree with ours to within 0.1 eV. Hilaire was the only one who produced PtO by heating in O_2 and could only produce it when another metal was present. Hammond and Kim both prepared PtO electrochemically. Hecq prepared PtO by sputtering deposition and Fleisch studied reduction of PtO powder. Our value of 72.3 eV does not agree with the values of Kim and Fleisch, but does agree with the others. Hammond also reported a binding energy of 72.4 eV for $Pt(OH)_2$ and a value of 72.3 eV for a surface Pt oxide species with a thickness of 8.0 Å or less and for the decomposition of PtO_2.

The presence of Ce with Pt is essential to produce a Pt chemical shift. This must be because Ce either stabilizes Pt oxide or catalyzes the oxidation of Pt. Others observed that Pt would remain metallic when alone and heated in O_2, but could oxidize if a sufficient amount of Pd, Ru, or Ir were present (*17*). They did not examine the effect of Ce, but our observation is consistent with theirs. Apparently, the presence of another metal which is more easily oxidized, including Ce, can facilitate oxidation of Pt. Others proposed oxidation of Pt on $Pt–Ce/Al_2O_3$ catalysts but did not show any direct evidence to confirm this conclusion (*28*). Summers and Ausen concluded that Ce promotes the oxidation of Pt based on infrared spectroscopic investigations of CO chemisorption over Pt and $Pt–Ce/Al_2O_3$ catalysts, but they did not present direct evidence of Pt oxidation, nor did they discuss the nature of the resulting oxide (*1*). Others have used Raman spectroscopy to confirm the existence of PtO (*29*) and concluded that highly dispersed Pt supported on γ-Al_2O_3 is present as an amorphous oxide after calcination (*30*), but these catalysts did not contain Ce. A study of Pt/CeO_2 catalysts showed the formation of Pt^{+2} by heating in O_2 at 373°K and reduction of the oxide by heating in vacuum at 800°K (*31*), but this was for a CeO_2 support, not Al_2O_3 or SiO_2.

Oxidation and Reduction of Ce

The major difference in the behavior of Ce on the two supports was that Ce formed an amorphous Ce^{+3} species following heating in H_2 on SiO_2 while it was always observed as crystalline CeO_2 on Al_2O_3. This does not rule out the possibility of Ce being effective for oxygen storage since CeO_2 could have reduced in H_2 and reoxidized in ambient air and since only a small fraction, about 1–2%, is active in oxygen storage, even in the presence of Pt or Rh (*32*).

Others have shown that Ce can form Ce_2O_3 on Al_2O_3 following heating in H_2 (*3*). Our observations are not necessarily inconsistent with these because we believe that Ce_2O_3 was probably formed in our samples upon heating in H_2 and oxidized after exposure to air at room temperature. The fact that we observe Ce_2O_3 on SiO_2 after heating in H_2 and exposure to air shows that Ce_2O_3 does not oxidize as easily on SiO_2 as it does on Al_2O_3.

Others have observed $CeAlO_3$ on CeO_2/Al_2O_3 samples by heating in H_2 at temperatures higher than 600°C (*9*). They state that Ce_2O_3 would not form because it is less thermodynamically stable than $CeAlO_3$ and that $CeAlO_3$ shows thermal stability in air up to 600°C. Since we did not observe $CeAlO_3$ in our samples after heating in H_2 at 650°C and exposure to ambient air, we conclude that we did not form significant $CeAlO_3$. This is consistent with their observations for CeO_2 particles, which they state would not form $CeAlO_3$ at reduction temperatures below 800°C. We have not studied this system at temperatures over 800°C where they were able to observe reduction of CeO_2 particles to $CeAlO_3$.

SUMMARY

Pt oxidizes in the presence of Ce to Pt^{+2} when heated in O_2. The presence of Ce sta-

bilizes the Pt oxide formed so that the loss of Pt due to volatilization of the oxide is slowed by the presence of Ce. Similar behavior is seen on both Al_2O_3 and SiO_2.

Unlike Rh–Ce/SiO_2, there is no redispersion of Rh_2O_3 on Al_2O_3 when heated in O_2 in the presence of Ce. Rh and Rh_2O_3 are much less mobile on Al_2O_3, making redispersion and sintering between particles impossible. However, on SiO_2, Rh_2O_3 spreads on the surface as a film. This allows for redispersion of Rh particles after heating in H_2 at low temperatures and sintering of Rh particles following heating at high temperatures.

Another difference between Rh–Ce/SiO_2 and Rh–Ce/Al_2O_3 is the formation of $Ce_2Si_2O_7$ on SiO_2 and the absence of $CeAlO_3$ on Al_2O_3 for comparable treatments. On SiO_2, Ce forms Ce_2O_3 following heating in H_2 which remains as Ce_2O_3 after exposure to air. On Al_2O_3, Ce probably forms Ce_2O_3 when heated in H_2, but oxidizes to CeO_2 upon exposure to ambient air. Ce will form CeO_2 following heating in O_2 on either support.

ACKNOWLEDGMENT

The assistance of Dr. R. A. Caretta in performing the XPS is greatly appreciated.

REFERENCES

1. Summers, J. C., and Ausen, S. A., *J. Catal.* **58,** 131 (1979).
2. Jin, T., Okuhara, T., Mains, G. J., and White, J. M., *J. Phys. Chem.* **91,** 3310 (1987).
3. Herz, R. K., *Ind. Eng. Chem. Prod. Res. Dev.* **20,** 451 (1981).
4. Cho, B. K., Shanks, B. H., and Bailey, J. E., *J. Catal.* **115,** 486 (1989).
5. Kim, G., *Ind. Eng. Chem. Prod. Res. Dev.* **21,** 267 (1982).
6. Schlatter, J. C., and Mitchell, P. J., *Ind. Eng. Chem. Prod. Res. Dev.* **19,** 288 (1980).
7. Harrison, B., Diwell, A. F., and Hallett, C., *Platinum Met. Rev.* **32,** 73 (1988).
8. Krause, K. R., Schabes-Retchkiman, P., and Schmidt, L. D., *J. Catal.* **134,** 204 (1992).
9. Shyu, J. Z., Weber, W. H., and Grandhi, H. S., *J. Phys. Chem.* **92,** 4964 (1988).
10. Yao, H. C., and Yu Yao, Y. F., *J. Catal.* **86,** 254 (1984).
11. Meriaudeau, P., Dutel, J. F., Dufaux, M., and Naccache, C., *in* "Metal–Support and Metal-Additive Effects in Catalysis" (B. Imelik *et al.*, Eds.), p. 95. Elsevier, Amsterdam, 1982.
12. Den Otter, G. J., and Dautzenberg, F. M., *J. Catal.* **53,** 116 (1978).
13. Chojnacki, T. P., Krause, K. R., and Schmidt, L. D., *J. Catal.* **128,** 161 (1991).
14. Wang, T., and Schmidt, L. D., *J. Catal.* **71,** 411 (1981).
15. Wagner, C. D., Riggs, W. M., Davis, L. E., Moulder, J. F., and Muilenberg, G. E., "Handbook of X-Ray Photoelectron Spectroscopy." Perkin–Elmer Corporation, Eden Prairie, MN, 1979.
16. Hammond, J. S., and Winograd, N., *J. Electroanal. Chem.* **78,** 55 (1977).
17. Hilaire, L., Diaz Guerrero, G., Legare, P., Maire, G., and Krill, G., *Surf. Sci.* **146,** 569 (1984).
18. Hecq, M., Hecq. A., Delrue, J. P., and Robert, T., *J. Less-Common Met.* **64,** P25 (1979).
19. Kim, K. S., Winograd, N., and Davis, R. E., *J. Am. Chem. Soc.* **93,** 6296 (1971).
20. Fleisch, T. H., and Mains, G. J., *J. Phys. Chem.* **90,** 5317 (1986).
21. Egerton, R. F., "Electron Energy-Loss Spectroscopy in the Electron Microscope." Plenum, New York, 1989.
22. Wang, T., Lee, C. P., and Schmidt, L. D., *Surf. Sci.* **163,** 181 (1985).
23. Lee, W. H., Vanloon, K. R. Petrova, V., Woodhouse, J. B., Loxton, C. M., and Masel, R. I., *J. Catal.* **126,** 658 (1990).
24. Berry, R. J., *Can. J. Chem.* **55,** 1792 (1977).
25. Fryburg, G. C., and Petrus, H. M., *J. Electrochem. Soc.* **108,** 496 (1961).
26. Chaston, J. C., *Platinum Met. Rev.* **19,** 135 (1975).
27. "Handbook of Chemistry and Physics" (R. C. Weast and M. J. Astle, Eds.), p. D-225. CRC Press, Boca Raton, FL, 1979.
28. Yu Yao, Y. F., *Ind. Eng. Chem. Prod. Res. Dev.* **19,** 293 (1980).
29. McBride, J. R., Graham, G. W., Peters, C. R., and Weber, W. H., *J. Appl. Phys.* **69,** 1596 (1991).
30. Graham, G. W., Weber, W. H., McBride, J. R., and Peters, C. R., *J. Raman Spectrosc.* **22,** 1 (1991).
31. Jin, T., Zhou, Y., Mains, G. J., and White, J. M., *J. Phys. Chem.* **91,** 5931 (1987).
32. Su, E. C., Montreuil, C. N., and Rothschild, W. G., *Appl. Catal.* **17,** 75 (1985).